Surface albedo decreases from anthropogenic impacts over High Mountain Asia with implications of positive radiative forcing feedbacks

Fadji Z. Maina[1,2*], Sujay V. Kumar[1], Chandana Gangodagamage[1]

[1] NASA Goddard Space Flight Center, Hydrological Sciences Laboratory, Greenbelt, Maryland, USA
[2] University of Maryland, Baltimore County, Goddard Earth Sciences Technology and Research Studies and Investigations, Baltimore, Maryland, USA

*Corresponding Author: fadjizaouna.maina@nasa.gov

Abstract

Human and climate induced land surface changes resulting from irrigation, snow cover decreases, and greening impact the radiative forcing by changing the surface albedo. Here we use a partial information decomposition approach and remote sensing data to quantify the effects of the changes in leaf area index, soil moisture, and snow cover on the surface albedo in High Mountain Asia (HMA), home to over a billion people, from 2003 to 2020. The study establishes strong evidence of anthropogenic agricultural water use over irrigated lands (e.g., Ganges-Brahmaputra) which causes the highest surface albedo decreases (≤1%/year). Greening and decreased snow cover from warming also drive changes in visible and near-infrared surface albedo in different areas of HMA. The significant role of human management and human-induced greening in influencing albedo suggests the potential of a positive feedback cycle where albedo decreases lead to increased evaporative demand and increased stress on water resources.

1. Introduction

Surface albedo, the ratio of the solar radiation reflected from the Earth's surface to the solar radiation incident upon it, is an essential variable determining the energy balance at the land surface[1,2], in turn influencing local and global climates. A decrease in surface albedo gives rise to a positive radiative forcing, which can counterbalance the negative radiative forcing created by carbon sequestration[3] and promote surface warming. Surface albedo also has an influence on the fraction of energy transformed into sensible and latent heat fluxes[4–6]. Variations of surface albedo are driven by the changes of Earth surface (vegetation, snow coverage, soil moisture, etc.), the solar illumination, and the zenith angle[7–12]. Also, vegetation phenology and seasonality of climate[13,14] exert influences on the albedo changes at longer timescales. Consequently, natural disturbances such as warming and human activities such as deforestation and irrigation could alter the surface albedo[15], often larger than the biogeophysical mechanisms acting on the radiation budgets at both surface and atmospheric levels[16–20]. Therefore, quantifying the drivers of surface albedo changes can provide critical inferences on land-use change impacts on the radiative forcing.

High-Mountain Asia (HMA, Figure 1) covering the Tibetan Plateau and its surroundings consists of densely populated hydrologic basins (e.g., Ganges-Brahmaputra and the Yangtze) serving over a billion people[30–33]. HMA basins play a critical role in sustaining the economy, agriculture, and energy of around 10 countries including China, Nepal, Bangladesh, India, Pakistan, and Afghanistan. Land structure heterogeneity over HMA is tremendous, with elevation ranging from the sea level to the world's highest point, different climatic conditions (westerlies and monsoons), footprints of human activities, and large variations in land cover types. HMA experiences strong changes of land surface characteristics caused by greening[34,35], decreases in snow[30], and irrigation[73]. Because greening changes the optical and structural properties of the vegetation canopy and increases the Leaf Area Index (LAI), it affects the surface albedos[25,36,37]. Decreases in cryospheric storages resulting from warming, changes of precipitation phases, and dust and black carbon deposits also contribute to surface albedo decreases[38–40]. Lastly, significant irrigation activities also influence surface albedo by decreasing ground reflectance and enhancing vegetation growth.

Quantifying the relationships between these cryospheric and biospheric changes and the surface albedo in HMA where land surface processes play a significant role in the hydrodynamics[41–43] will provide a better understanding of (1) their impacts on the climate system and water resources[44,45], (2) the impacts of land surface changes on the radiative forcing, crucial for designing climate change mitigation and adaptation strategies[46–48], and (3) the contributions of human management to Earth's warming and/or cooling. Even though irrigation, warming, and greening are occurring at high rates in HMA, previous studies assessing surface albedo changes were limited to the Tibetan Plateau[49,50] and the Himalayas[39].

Satellite remote sensing is an essential technique for estimating surface albedo at various spectral, spatial, and temporal resolutions[22]. Examining the broadband components of surface albedo such as visible radiation (VIS) with a wavelength between 0.3 and 0.7 μm and near-infrared radiation (NIR) with a wavelength between 0.7 and 5.0 μm[22,23] allows assessing changes in different land surface and vegetation states. For example, vegetation canopies reflect a much larger fraction in the NIR than in the VIS, because plant canopies scatter NIR energy[24,25,26] whereas the VIS has a stronger correlation with the soil moisture and snow cover[19,27–29]. Here, we rely on a partial information decomposition analysis with remote sensing data to quantify the impacts of changes in (1) LAI, (2) soil moisture, and (3) snow cover on the black sky and white sky surface albedos in VIS and NIR broadband over HMA from 2003 to 2020. We use the albedo climatology provided by MODIS V006 (MCD43A3[51]), LAI provided by MCD15A2H Version 6 of MODIS[52], snow cover fraction provided by MODIS MOD10CM[53], and soil moisture provided by the European Space Agency Climate Change Initiative ESA CCI[54].

Based on the analysis of remote sensing datasets of surface albedo and other land surface variables, this study establishes strong evidence of anthropogenic agricultural water use, with implications for the development of positive radiative forcing in HMA[79]. Specifically, the study demonstrates that increases in soil moisture in irrigated lands (Ganges-Brahmaputra and Indus) drive the highest decreases in surface albedo. Soil moisture drives the reductions in surface albedo in non-irrigated lands of the Indus and the northern HMA while the declines in snow cover from warming decrease surface albedos in the Tibetan Plateau. Although warming, dust, and black carbon induced snow cover decreases exert an influence of the positive radiative forcing, these impacts are limited to the water towers and the winter season. While greening enhances NIR and decreases VIS in snow-free forests (e.g., Yangtze), in snow-covered vegetated areas (e.g., Himalayas, Amu Darya, and Hwang Ho), it increases both the VIS and the NIR. In addition to the established snow albedo feedback where the reduction in surface albedo over snow-covered areas leads to increased net radiation and sustained melt[75], the current study outlines another possible positive feedback cycle related to surface albedo. In densely populated areas downstream of the high elevation mountains, human management, and human-induced greening dominate the highest decreases in surface albedo (up to 1%/year), which can lead to increases in the evaporative demand and subsequent increased irrigation water use in a positive feedback cycle. The increased stress on the limited water resources in this region from such impacts is a significant concern. These anthropogenic amplifications should be accounted for in climate modeling studies and in designing mitigation strategies for managing the impacts on the water cycle.

2. Results

2.1. Surface albedo changes in HMA

Forested basins (Yangtze, Si, Song Hong, and Irrawaddy) have the lowest surface albedos due to their dense canopy (Figure 2). The highest surface albedos (NIR >0.35 and VIS >0.2) are in the Himalayas and the northern HMA due to the presence of snow. In the irrigated lands of Indus and Ganges-Brahmaputra, surface albedo values are in between those of forests and bare soil. Surface albedo trends are bidirectional although the VIS has a decreasing trend almost everywhere (Figure 2). The irrigated lands and Hwang Ho have the highest decreases in both NIR and VIS ($> -2.10^{-3}$/year). The northwestern basins have an increasing trend in NIR ($>10^{-3}$/year) whereas some areas show no significant trends to increasing trends of VIS. Tarim and the northern HMA are characterized by decreasing trends in NIR ($<10^{-3}$/year) and VIS ($\sim -2.10^{-3}$/year). Forested basins show an increasing trend in NIR (~10^{-3}/year) and a decreasing trend in VIS (from 10^{-4} to 10^{-3}/year). Previous studies have reported an increasing trend of surface albedo in central Asia[55] in general and a decreasing trend in the Tibetan Plateau[49,50] whereas our study highlights that these trends are bidirectional in the surface albedos constituents.

Trends of snow cover and LAI are unidirectional with decreasing and increasing trends respectively, whereas the soil moisture has a bidirectional trend (Supplementary Figure 1). Forests have the highest LAI increase and snow cover decrease yet they depict low surface albedo changes. Moreover, Hwang Ho and Tarim characterized by high surface albedos changes do not have large changes of LAI, snow cover, and soil moisture. The long-term patterns of surface albedo changes are, therefore, not explained by the changes in vegetation, snow, and soil moisture alone. This following section describes the key land surface processes and their interactions on influencing albedo.

2.2.Drivers of surface albedo changes in HMA

Figure 3 which shows the unique, synergistic, and redundant information in various drivers of surface albedo changes, indicates that these factors are spatiotemporally heterogeneous in HMA. The unique information from soil moisture, LAI, or snow cover dominates the surface albedo, though in some instances the redundant information across these variables also becomes important. The synergistic information across these factors is generally small. Overall, LAI is the main driver of surface albedo changes in HMA as it dominates the surface albedo changes in forested and northwestern basins. Due to intense irrigation activities, soil moisture is the primary factor influencing surface albedo changes over the irrigated lands of Indus and Ganges-Brahmaputra. For example, the unique information of soil moisture is three to four times higher than those of LAI and snow cover in Indus and Ganges-Brahmaputra. Compared to different areas of HMA, the redundant information between LAI and soil moisture is non-significant over Indus and Ganges-Brahmaputra basins, which reaches a peak in July when the high soil moisture interferes with the soil reflectance by decreasing the VIS component. Further, the enhanced vegetation growth also leads to increasing NIR. LAI is the dominant factor with large unique information in the forested areas of Irrawaddy, Song Hong, and Si; this influence progressively reduces depending on the density of the forest canopy (68% in Irrawaddy, 56% in Song Hong, and 32% in Si). Though the unique information of soil moisture is low in these areas, it increases during the monsoon. Snow is a significant factor in influencing the surface albedo in the Tibetan Plateau, the Karakoram and the western Himalayas, and the central Ganges-Brahmaputra and Eastern Himalayas. There is a seasonality to the snow cover unique information which increases in winter. The contrasting seasonal influences of snow cover, soil moisture, and LAI are also observed in several areas. Because multiple processes govern the water and energy balances in the central and eastern Himalayas, Hwang Ho, Tarim, and the northwestern basins (Amu Darya, Syr Darya, and Ili), surface albedo changes in these zones have multiple drivers whose contributions are seasonally dependent. In the Hwang Ho and Yangtze, for example, surface albedo variations are primarily governed by the changes of LAI though snow cover has a non-trivial contribution in winter. Additionally, soil moisture changes in Hwang Ho also affect surface albedo because its vegetated areas (48% of the basin area) are not dense enough to absorb all the solar radiation, hence nonnegligible radiation reaches the soil. In the central and eastern Himalayas, the unique information of LAI and soil moisture peaks in July. Because the increases in soil moisture are due to snowmelt, the unique information of snow cover and soil moisture have opposite monthly variations. During the growing season, the unique information of LAI is two times higher than those of snow cover and soil moisture combined. The partial information analysis presented here provides important insights about the key processes that drive the surface albedo and the subsequent radiative changes in HMA basins. Next, we describe the seasonal and long-term changes in these processes toward influencing surface albedo changes over HMA.

2.2.1. Irrigation induces the highest surface albedo decreases in HMA

The Ganges-Brahmaputra and the Indus are subject to agricultural activities involving intense irrigation[56] and groundwater pumping[57]. Irrigated lands occupy 49% of the Ganges-Brahmaputra and 22% of the Indus. They have the highest yearly decreases in VIS and NIR in HMA on average equal to -4.4 10^{-4}/year and -2 10^{-4}/year, respectively in the Ganges-Brahmaputra and -6 10^{-4}/year for the VIS and -2 10^{-4}/year for the NIR in the Indus. The highest yearly decreases in VIS and NIR are from February to June when the soil moisture increases significantly (Figure 4a). In the average seasonal cycle, the VIS increases from January to April because of the decreases in LAI and soil moisture. As soil moisture and LAI keep decreasing to reach their lowest values, the VIS reaches its maximum value (0.1) in June (Figure 4a). The beginning of the rainy season triggers increases in soil moisture and LAI. Hence the VIS starts to decrease. With the increases in LAI, more incoming solar energy is reflected and scattered by the vegetation canopy and only a small proportion of the incoming radiation reaches the ground[73]. The VIS remains at its lowest value (~0.05) for two consecutive months August and September when the average LAI and soil moisture have their highest values 2.5 and 0.29 respectively. The NIR has a monthly variation analogous to that of LAI because of its sensitivity to vegetation reflectance. Though not from irrigation, the influence of soil moisture on albedo is also seen in other areas. In the northern HMA and parts of Indus, soil moisture increases originating from increases in precipitation[77] decrease the surface albedo at rates equal to -2.3 10^{-4}/year for the VIS and -1.6 10^{-4}/year for the NIR (Supplementary Figure 4).

2.2.2. Greening decreases the VIS and increases the NIR surface albedo over forested regions of HMA

Though HMA experiences greening at high rates[73], LAI only controls surface albedo changes in forests of Ganges-Brahmaputra, Yangtze, Irrawaddy, Song Hong, and Si. Because of its dense canopy and high precipitation (970 to 1200 mm/year) leading to high soil moisture, annual averages of NIR and VIS surface albedos in the Yangzte are low equal to 0.275 and 0.187 respectively (Figure 4b). The Yangtze has one of the highest trends of LAI in HMA (up to 0.02 m^2m^{-2}/year). Nevertheless, the surface albedo trends are low likely due to their small magnitudes. The VIS and NIR surface albedos have contrasting trends and monthly variations due to the presence of forests. The VIS is high in winter due to vegetation senescence with a peak in March while the NIR component becomes high in summer. The lowest VIS (0.05) is from May to August when LAI and soil moisture are high, and snow cover low. VIS decreases as the canopy becomes dense and the wetness of the soil increases to dampen the effects of ground reflectance. As the canopy develops, its NIR reflectance increases due to increased multiple scattering[74]. Similar patterns are found in the forested areas of Ganges-Brahmaputra and Irrawaddy. Ganges-Brahmaputra forests are characterized by a low VIS (0.027, Supplementary Figure 2b). The yearly increasing trends of LAI cause the NIR to increase ($6\ 10^{-4}$/year) and the VIS to decrease ($-2.8\ 10^{-4}$/year), consistent with prior studies[59]. In the Irrawaddy, greening increases the NIR (up to $4\ 10^{-4}$/year) and decreases the VIS (Supplementary Figure 3a). In these domains, the pattern of monthly variations of trends and seasonality in LAI and soil moisture is similar. Consequently, the pattern of their impacts on surface albedo components is also similar.

2.2.3. Snow cover dominates surface albedo changes in high-elevation zones

Snow cover drives surface albedos changes in the Tibetan Plateau, the Karakoram, and the western Himalayas. The latter has an overall increasing trend of surface albedo stemming from an increasing snow cover (Figure 4c). However, this increasing trend is only limited to the winter, as surface albedo has a decreasing trend in summer and fall (Supplementary Figure 7) likely because of dust and black carbon deposits that darken the snow[38,39,60]. Similar patterns are also observed in the Tibetan plateau, where surface albedo decreases because of the decrease in snow cover (Supplementary Figure 5). The latter has also been attributed to black carbon[40] and greening in prior studies[50,61]. The albedo decrease from snow cover influence is, therefore, strongly related to human impacts and climate induced warming on snow cover.

2.2.4. Interactions between decreases in snow cover, increase in soil moisture, and greening

In a number of basins in HMA, the simultaneous influence of the changes in snow cover, soil moisture, and vegetation impacts surface albedo changes. For example, because all the three factors controlling surface albedos are preponderant, the Hwang Ho has one of the highest decreasing trends of NIR and VIS in HMA equal to 5 10^{-4}/year. In the Hwang Ho, the VIS decreases from January to August to reach its lowest value (~0.08) then increases as the winter season begins on contrary to the NIR (Figure 5a). In the Tarim, the decreasing trends of NIR and VIS (>-2 10^{-4}/year) are due to the decreasing trends of snow cover in winter and soil moisture and LAI from April to November (Supplementary Figure 5). In the Amu Darya and the other northwestern basins, the NIR has an increasing yearly trend and the VIS has an increasing trend due to the yearly increase in LAI (Figure 5b). The increases in VIS are also related to the decreasing trends of soil moisture (Supplementary Figure 6).

Decreases in surface albedo equal to -4 10^{-4}/year and -8 10^{-5}/year for NIR and VIS, respectively in the central and eastern Himalayas characterized by high VIS (0.09) and low NIR (0.11) are governed by LAI, soil moisture, and snow cover (Supplementary Figure 2a). Although surface albedo is decreasing over the years, in winter it is increasing likely because greening enhances snow interception. In forests where snowfall occurs, the canopy increases both VIS and NIR because the intercepted snow offsets the canopy reflectance in all wavelengths[58]. The NIR and VIS increase from January to reach their peak in March as the snow cover is high. As the canopy becomes snow-free and it starts reflecting in the NIR. As such, the decreases in NIR due to the decline of snow are compensated with the increases induced by the canopy reflectance. Therefore, the decreases in NIR are not as sharp as in the VIS. The NIR and VIS increase again in November when the winter begins. Due to the opposite effects of snow and forests on the NIR, the second increase is only detectible in the VIS (Supplementary Figure 2).

3. Discussion

Because irrigated lands have the highest surface albedo decreases, irrigation in HMA could significantly reshape its climate dynamics. Surface albedo decreases driven by human management are likely to have a positive feedback impact on water resource requirements. For example, the reduction in surface albedo due to irrigation could lead to more warming and high evaporative demand, which could subsequently lead to more irrigation demand and the overuse of water resources. Over the Ganges-Brahmaputra and Indus with large populations reliant on irrigated agriculture, these surface albedo decreases are a significant concern. Another positive feedback mechanism related to cold season processes also raises concerns about the shifts in water availability. Surface albedo changes derived from the decreases in snow will further enhance this decrease in snowpack and warming. A decrease in surface albedo increases the surface absorption of the solar radiation, leading to decreases in snow and more water available for vegetation growth and, therefore, boosts greening. In snow-covered forests, on the other hand, greening increases surface albedo and could attenuate warming. The impacts of the changes of land surface features (irrigation, greening, decreases in snow) on the radiative forcing will in turn accentuate these changes and the practices that have caused them. The attributions of the surface albedo changes developed in this study, therefore, are important inferences for future modeling studies for representing these interactions and feedbacks and evaluating their role in climate change. It is also important to account for this feedback in designing climate change mitigation strategies as counterbalancing Earth's warming could involve changes of practices such as irrigation.

4. Methods

4.1. Selected satellite-based products

We use remote sensing datasets to quantify the changes in surface albedo, LAI, soil moisture, and snow cover.

MODIS MCD43 surface albedo: We use the surface albedos provided by NASA's MODIS version V006 (MCD43A3) and their associated quality layers[62]. MODIS surface albedo products are generated every 8 days and have a spatial resolution of approximately 500 m. MCD43 provides BSA (directional hemispherical reflectance) which described the albedo under direct illumination condition in the absence of a diffuse component (i.e., when the sun as a point of source of illumination) and WSA (bihemispherical reflectance) is defined as albedo in the absence of a direct component when the diffuse component is isotropic in NIR and VIS.

MODIS MCD14A2H LAI: LAI, defined as the area of green leaves per unit ground horizontal surface area, is a good indicator of changes in vegetation greenness on Earth. LAI is widely used to analyze greening on Earth[63,64]. We use the LAI values provided by the MCD15A2H Version 6 of MODIS[52] at a spatial resolution of 500 m and a temporal resolution equal to 8 days.

MODIS Snow Cover fraction: we assess the monthly snow cover fraction estimates provided by MODIS Snow Cover fraction L3 at a spatial resolution of 0.05°[53].

ESA CCI Soil moisture: we analyze the daily soil moisture provided by the European Space Agency Climate Change Initiative ESA CCI[54]. The ESA CCI soil moisture v05.2 consists of three surface soil moisture data sets. In this study, we use the dataset generated by blending the soil moisture retrievals from active and passive microwave remote sensing instruments.

Statistical analyses

To capture the influence of HMA heterogeneity on albedo changes, we perform our analysis at 500 m, which is the spatial resolution of the surface albedo data. The changes of surface albedo and its potential control variables (LAI, snow cover, and soil moisture) over the past two decades are quantified by computing their trends using the Mann-Kendall test with a confidence level of 95%[70–72] given by:

$$S = \sum_{i=1}^{n-1} \sum_{j=k+1}^{n} sign(x_j - x_i) \quad (1)$$

where x is the time series variable. The subscript j and k are the observation time. $sign(x_j - x_i)$is equal to +1, 0, or -1, which means increasing, no, and decreasing trends, respectively.

Because three variables are likely controlling the changes of surface albedo, we employ the partial information decomposition framework to quantify the interactions and dependencies between these variables and the surface albedo. The partial information decomposition allows to quantify (1) the amount of information that each control variable uniquely contributes to the surface albedo, (2) the redundant information between the three variables, and (3) the information due to the combined knowledge of the three variables called synergistic information. More details about the computation of these metrics can be found in[69–71]. Land surface processes are characterized by strong seasonality and depending on the season the dominant factors, as well as the values of surface albedos, may change[16,19], we, therefore, analyze the monthly variations of yearly trends and averages.

Data availability

Datasets used in this study can be found in the following websites:

MODIS Albedo: https://lpdaac.usgs.gov/products/mcd43a3v006/

MODIS LAI: https://lpdaac.usgs.gov/products/mcd15a2hv006/

MODIS Snow Cover: https://nsidc.org/data/MOD10A1

ESA CCI soil moisture: https://www.esa-soilmoisture-cci.org/data

GRACE data: https://grace.jpl.nasa.gov/data/get-data/jpl_global_mascons/

Author contribution

F.Z.M and S.V.K. contributed with conceptualization, data analysis, and writing.

C.G. contributed with the data acquisition.

S.V.K. was responsible for funding acquisition. All authors have read and agreed to the published version of the manuscript.

Competing interests

The authors declare that they have no conflict of interest.

Acknowledgements

This research was supported by the grant from the National Aeronautics and Space Administration High Mountain Asia program (19-HMA19-0012). Computing was supported by the resources at the NASA Center for Climate Simulation.

References

1. Dickinson, R. E. Land Surface Processes and Climate—Surface Albedos and Energy Balance. in *Advances in Geophysics* (ed. Saltzman, B.) vol. 25 305–353 (Elsevier, 1983).
2. Liang, S., Wang, K., Zhang, X. & Wild, M. Review on Estimation of Land Surface Radiation and Energy Budgets From Ground Measurement, Remote Sensing and Model Simulations. *IEEE J. Sel. Top. Appl. Earth Obs. Remote Sens.* **3**, 225–240 (2010).
3. Betts, R. A. Offset of the potential carbon sink from boreal forestation by decreases in surface albedo. *Nature* **408**, 187–190 (2000).
4. Wang, S., Grant, R. F., Verseghy, D. L. & Black, T. A. Modelling carbon-coupled energy and water dynamics of a boreal aspen forest in a general circulation model land surface scheme. *Int. J. Climatol.* **22**, 1249–1265 (2002).
5. Wang, S., Grant, R. F., Verseghy, D. L. & Black, T. A. Modelling plant carbon and nitrogen dynamics of a boreal aspen forest in CLASS — the Canadian Land Surface Scheme. *Ecol. Model.* **142**, 135–154 (2001).
6. Zhao, K. & Jackson, R. B. Biophysical forcings of land-use changes from potential forestry activities in North America. *Ecol. Monogr.* **84**, 329–353 (2014).
7. Gao, F. *et al.* MODIS bidirectional reflectance distribution function and albedo Climate Modeling Grid products and the variability of albedo for major global vegetation types. *J. Geophys. Res. Atmospheres* **110**, (2005).
8. Kuusinen, N., Tomppo, E., Shuai, Y. & Berninger, F. Effects of forest age on albedo in boreal forests estimated from MODIS and Landsat albedo retrievals. *Remote Sens. Environ.* **145**, 145–153 (2014).

9. Lukeš, P., Rautiainen, M., Manninen, T., Stenberg, P. & Mõttus, M. Geographical gradients in boreal forest albedo and structure in Finland. *Remote Sens. Environ.* **152**, 526–535 (2014).

10. Rechid, D., Raddatz, T. J. & Jacob, D. Parameterization of snow-free land surface albedo as a function of vegetation phenology based on MODIS data and applied in climate modelling. *Theor. Appl. Climatol.* **95**, 245–255 (2009).

11. Wang, S. Dynamics of surface albedo of a boreal forest and its simulation. *Ecol. Model.* **183**, 477–494 (2005).

12. Wang, Z. *et al.* Using MODIS BRDF and Albedo Data to Evaluate Global Model Land Surface Albedo. *J. Hydrometeorol.* **5**, 3–14 (2004).

13. Richardson, A. D. *et al.* Climate change, phenology, and phenological control of vegetation feedbacks to the climate system. *Agric. For. Meteorol.* **169**, 156–173 (2013).

14. Wang, S. & Davidson, A. Impact of climate variations on surface albedo of a temperate grassland. *Agric. For. Meteorol.* **142**, 133–142 (2007).

15. He, T., Liang, S. & Song, D.-X. Analysis of global land surface albedo climatology and spatial-temporal variation during 1981–2010 from multiple satellite products. *J. Geophys. Res. Atmospheres* **119**, 10,281-10,298 (2014).

16. Abera, T. A., Heiskanen, J., Pellikka, P., Rautiainen, M. & Maeda, E. E. Clarifying the role of radiative mechanisms in the spatio-temporal changes of land surface temperature across the Horn of Africa. *Remote Sens. Environ.* **221**, 210–224 (2019).

17. Alkama, R. & Cescatti, A. Biophysical climate impacts of recent changes in global forest cover. *Science* **351**, 600–604 (2016).

18. Laguë, M. M. & Swann, A. L. S. Progressive Midlatitude Afforestation: Impacts on Clouds, Global Energy Transport, and Precipitation. *J. Clim.* **29**, 5561–5573 (2016).

19. Roesch, A., Wild, M., Pinker, R. & Ohmura, A. Comparison of spectral surface albedos and their impact on the general circulation model simulated surface climate. *J. Geophys. Res. Atmospheres* **107**, ACL 13-1-ACL 13-18 (2002).

20. Wielicki, B. A. *et al.* Changes in Earth's Albedo Measured by Satellite. *Science* **308**, 825–825 (2005).

21. Bonan, G. *Ecological Climatology: Concepts and Applications*. (Cambridge University Press, 2015). doi:10.1017/CBO9781107339200.

22. He, T. *et al.* Estimation of surface albedo and directional reflectance from Moderate Resolution Imaging Spectroradiometer (MODIS) observations. *Remote Sens. Environ.* **119**, 286–300 (2012).

23. Shuai, Y. *et al.* Re-understanding of land surface albedo and related terms in satellite-based retrievals. *Big Earth Data* **4**, 45–67 (2020).

24. Zheng, L. *et al.* Spatial, temporal, and spectral variations in albedo due to vegetation changes in China's grasslands. *ISPRS J. Photogramm. Remote Sens.* **152**, 1–12 (2019).

25. Alibakhshi, S., Hovi, A. & Rautiainen, M. Temporal dynamics of albedo and climate in the sparse forests of Zagros. *Sci. Total Environ.* **663**, 596–609 (2019).

26. Hovi, A. *et al.* Seasonal dynamics of albedo across European boreal forests: Analysis of MODIS albedo and structural metrics from airborne LiDAR. *Remote Sens. Environ.* **224**, 365–381 (2019).

27. Carrer, D. *et al.* Dynamic mapping of snow-free vegetation and bare soil albedos at global 1km scale from 10-year analysis of MODIS satellite products. *Remote Sens. Environ.* **140**, 420–432 (2014).

28. Qu, X. & Hall, A. What Controls the Strength of Snow-Albedo Feedback? *J. Clim.* **20**, 3971–3981 (2007).

29. Yang, J., Li, Z., Zhai, P., Zhao, Y. & Gao, X. The influence of soil moisture and solar altitude on surface spectral albedo in arid area. *Environ. Res. Lett.* **15**, 035010 (2020).

30. Immerzeel, W. W., Beek, L. P. H. van & Bierkens, M. F. P. Climate Change Will Affect the Asian Water Towers. *Science* **328**, 1382–1385 (2010).

31. Pritchard, H. D. Asia's shrinking glaciers protect large populations from drought stress. *Nature* **569**, 649–654 (2019).

32. Qiu, J. China: The third pole. *Nature* **454**, 393–396 (2008).

33. Viviroli, D., Dürr, H. H., Messerli, B., Meybeck, M. & Weingartner, R. Mountains of the world, water towers for humanity: Typology, mapping, and global significance. *Water Resour. Res.* **43**, (2007).

34. Chen, C. *et al.* China and India lead in greening of the world through land-use management. *Nat. Sustain.* **2**, 122–129 (2019).

35. Zhang, Y. *et al.* Multiple afforestation programs accelerate the greenness in the 'Three North' region of China from 1982 to 2013. *Ecol. Indic.* **61**, 404–412 (2016).

36. Alibakhshi, S., Naimi, B., Hovi, A., Crowther, T. W. & Rautiainen, M. Quantitative analysis of the links between forest structure and land surface albedo on a global scale. *Remote Sens. Environ.* **246**, 111854 (2020).

37. Bright, R. M., Zhao, K., Jackson, R. B. & Cherubini, F. Quantifying surface albedo and other direct biogeophysical climate forcings of forestry activities. *Glob. Change Biol.* **21**, 3246–3266 (2015).

38. Gautam, R., Hsu, N. C., Lau, W. K.-M. & Yasunari, T. J. Satellite observations of desert dust-induced Himalayan snow darkening. *Geophys. Res. Lett.* **40**, 988–993 (2013).
39. Sarangi, C. *et al.* Dust dominates high-altitude snow darkening and melt over high-mountain Asia. *Nat. Clim. Change* **10**, 1045–1051 (2020).
40. Wang, Z., Zhang, H. & Shen, X. Radiative forcing and climate response due to black carbon in snow and ice. *Adv. Atmospheric Sci.* **28**, 1336–1344 (2011).
41. Immerzeel, W. W., Beek, L. P. H. van & Bierkens, M. F. P. Climate Change Will Affect the Asian Water Towers. *Science* **328**, 1382–1385 (2010).
42. Loomis, B. D. *et al.* Water Storage Trends in High Mountain Asia. *Front. Earth Sci.* **7**, (2019).
43. Yoon, Y. *et al.* Evaluating the Uncertainty of Terrestrial Water Budget Components Over High Mountain Asia. *Front. Earth Sci.* **7**, (2019).
44. Barnes, C. & Roy, D. P. Radiative forcing over the conterminous United States due to contemporary land cover land use albedo change. *Geophysical Research Letters* vol. 35 (2008).
45. Bounoua, L., DeFries, R., Collatz, G. J., Sellers, P. & Khan, H. Effects of Land Cover Conversion on Surface Climate. *Clim. Change* **52**, 29–64 (2002).
46. Betts, R. A. Offset of the potential carbon sink from boreal forestation by decreases in surface albedo. *Nature* **408**, 187–190 (2000).
47. Bonan, G. B., Pollard, D. & Thompson, S. L. Effects of boreal forest vegetation on global climate. *Nature* **359**, 716–718 (1992).
48. Zeng, Z. *et al.* Climate mitigation from vegetation biophysical feedbacks during the past three decades. *Nat. Clim. Change* **7**, 432–436 (2017).

49. Tian, L., Chen, J. & Zhang, Y. Growing season carries stronger contributions to albedo dynamics on the Tibetan plateau. *PLOS ONE* **12**, e0180559 (2017).

50. Tian, L., Zhang, Y. & Zhu, J. Decreased surface albedo driven by denser vegetation on the Tibetan Plateau. *Environ. Res. Lett.* **9**, 104001 (2014).

51. Schaaf, Crystal & Wang, Zhuosen. MCD43A2 MODIS/Terra+Aqua BRDF/Albedo Quality Daily L3 Global - 500m V006. (2015) doi:10.5067/MODIS/MCD43A2.006.

52. Myneni, Ranga, Knyazikhin, Yuri & Park, Taejin. MOD15A2H MODIS/Terra Leaf Area Index/FPAR 8-Day L4 Global 500m SIN Grid V006. (2015) doi:10.5067/MODIS/MOD15A2H.006.

53. Hall, Dorothy, George, K., Riggs, A. & Salomonson, Vincent V. MODIS/Terra Snow Cover 5-Min L2 Swath 500m, Version 5. (2006) doi:10.5067/ACYTYZB9BEOS.

54. Dorigo, W. *et al.* ESA CCI Soil Moisture for improved Earth system understanding: State-of-the art and future directions. *Remote Sens. Environ.* **203**, 185–215 (2017).

55. Li, Q., Ma, M., Wu, X. & Yang, H. Snow Cover and Vegetation-Induced Decrease in Global Albedo From 2002 to 2016. *J. Geophys. Res. Atmospheres* **123**, 124–138 (2018).

56. Salmon, J. M., Friedl, M. A., Frolking, S., Wisser, D. & Douglas, E. M. Global rain-fed, irrigated, and paddy croplands: A new high resolution map derived from remote sensing, crop inventories and climate data. *Int. J. Appl. Earth Obs. Geoinformation* **38**, 321–334 (2015).

57. Water Home. https://www.worldbank.org/en/topic/water.

58. Moody, E. G., King, M. D., Schaaf, C. B., Hall, D. K. & Platnick, S. Northern Hemisphere five-year average (2000–2004) spectral albedos of surfaces in the presence of snow: Statistics computed from Terra MODIS land products. *Remote Sens. Environ.* **111**, 337–345 (2007).

59. Lukeš, P., Stenberg, P. & Rautiainen, M. Relationship between forest density and albedo in the boreal zone. *Ecol. Model.* **261–262**, 74–79 (2013).

60. Ming, J. *et al.* Widespread Albedo Decreasing and Induced Melting of Himalayan Snow and Ice in the Early 21st Century. *PLOS ONE* **10**, e0126235 (2015).

61. Tian, L., Chen, J. & Shao, C. Interdependent Dynamics of LAI-Albedo across the Roofing Landscapes: Mongolian and Tibetan Plateaus. *Remote Sens.* **10**, 1159 (2018).

62. Schaaf, Crystal & Wang, Zhuosen. MCD43A3 MODIS/Terra+Aqua BRDF/Albedo Daily L3 Global - 500m V006. (2015) doi:10.5067/MODIS/MCD43A3.006.

63. Piao, S. *et al.* Characteristics, drivers and feedbacks of global greening. *Nat. Rev. Earth Environ.* **1**, 14–27 (2020).

64. Zhu, Z. *et al.* Greening of the Earth and its drivers. *Nat. Clim. Change* **6**, 791–795 (2016).

65. Müller Schmied, H. *et al.* Variations of global and continental water balance components as impacted by climate forcing uncertainty and human water use. *Hydrol. Earth Syst. Sci.* **20**, 2877–2898 (2016).

66. Kendall, M. G. *Rank correlation methods*. (Griffin, 1948).

67. Mann, H. B. Nonparametric Tests Against Trend. *Econometrica* **13**, 245–259 (1945).

68. Yue, S., Pilon, P. & Cavadias, G. Power of the Mann–Kendall and Spearman's rho tests for detecting monotonic trends in hydrological series. *J. Hydrol.* **259**, 254–271 (2002).

69. Infotheory. http://mcandadai.com/infotheory/measures.html#pid_title.

70. Timme, N., Alford, W., Flecker, B. & Beggs, J. M. Synergy, redundancy, and multivariate information measures: an experimentalist's perspective. *J. Comput. Neurosci.* **36**, 119–140 (2014).

71. Williams, P. L. & Beer, R. D. Nonnegative Decomposition of Multivariate Information. *ArXiv10042515 Math-Ph Physicsphysics Q-Bio* (2010).

72. Friedl, Mark & Sulla-Menashe, Damien. MCD12Q1 MODIS/Terra+Aqua Land Cover Type Yearly L3 Global 500m SIN Grid V006. (2019) doi:10.5067/MODIS/MCD12Q1.006.

73. Maina, F.Z., Kumar, S.V., Albergel, C. et al. Warming, increase in precipitation, and irrigation enhance greening in High Mountain Asia. Commun Earth Environ 3, 43 (2022). https://doi.org/10.1038/s43247-022-00374-0

74. D.M. Gates, H.J. Keegan, J.C. Schleter, V.R. Weidner Spectral properties of plants *Appl. Opt., 4* (1965), pp. 11-20

75. Flanner, Mark G., et al. "Radiative forcing and albedo feedback from the Northern Hemisphere cryosphere between 1979 and 2008." Nature Geoscience 4.3 (2011): 151-155.

Figure caption

Figure 1: Maps of High Mountain Asia. (a) elevation, (b) land cover[76], and (c) percent of irrigated areas per pixel[56]. The black lines indicate the limits of the hydrologic basins, and their names are indicated in (c).

Figure 2: Surface albedo changes and values in High Mountain Asia. Spatial distributions of the yearly (a) averages and (b) trends from 2003 to 2020 of BSA (Black Sky) and WSA (White Sky) surface albedos in both NIR and VIS wavelengths. Trends were computed using the Mann-Kendall test with a confidence level of 95%.

Figure 3: Dominant drivers of the surface albedo changes. Spatiotemporal variations of the unique and redundant information of leaf area index, soil moisture, and snow cover about the visible white-sky surface albedo of 16 zones (basin names are indicated in Figure 1c). Note that y-axis is a stacked graph and is not cumulative.

Figure 4: Monthly variations of trends and averages of surface albedo, LAI, soil moisture and snow cover. (a) in a basin where irrigation decreases surface albedo: irrigated lands of the Ganges-Brahmaputra, (b) in a basin where greening decreases VIS and increases NIR surface albedo: Yangtze, (c) in a basin where changes in snow cover decreases surface albedo: the Karakoram and Western Himalayas in the Indus. Trends were computed using the Mann-Kendall test with a confidence level of 95%.

Figure 5: Monthly variations of trends and averages of surface albedo, LAI, soil moisture and snow cover in basins where surface albedo changes are controlled by greening, soil moisture, and snow cover (a) Hwang Ho, and (b) Amu Darya. Trends were computed using the Mann-Kendall test with a confidence level of 95%.

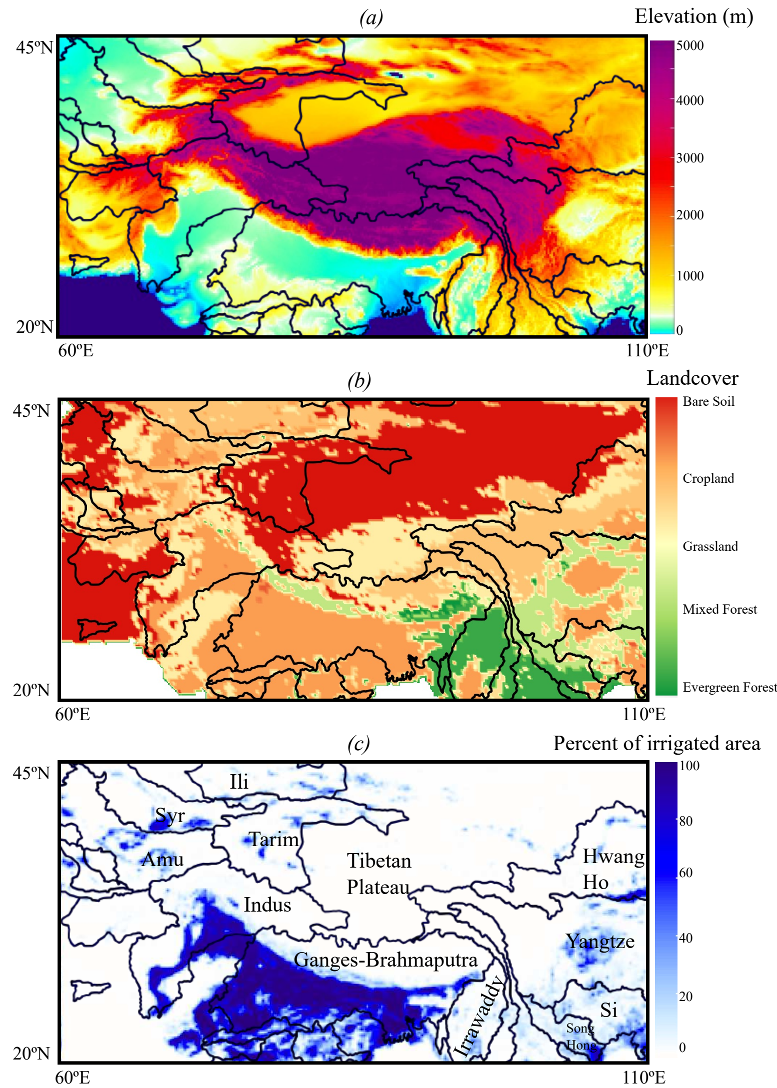

Figure 1: Maps of High Mountain Asia. (a) elevation, (b) land cover[76], and (c) percent of irrigated areas per pixel[56]. The black lines indicate the limits of the hydrologic basins, and their names are indicated in (c).

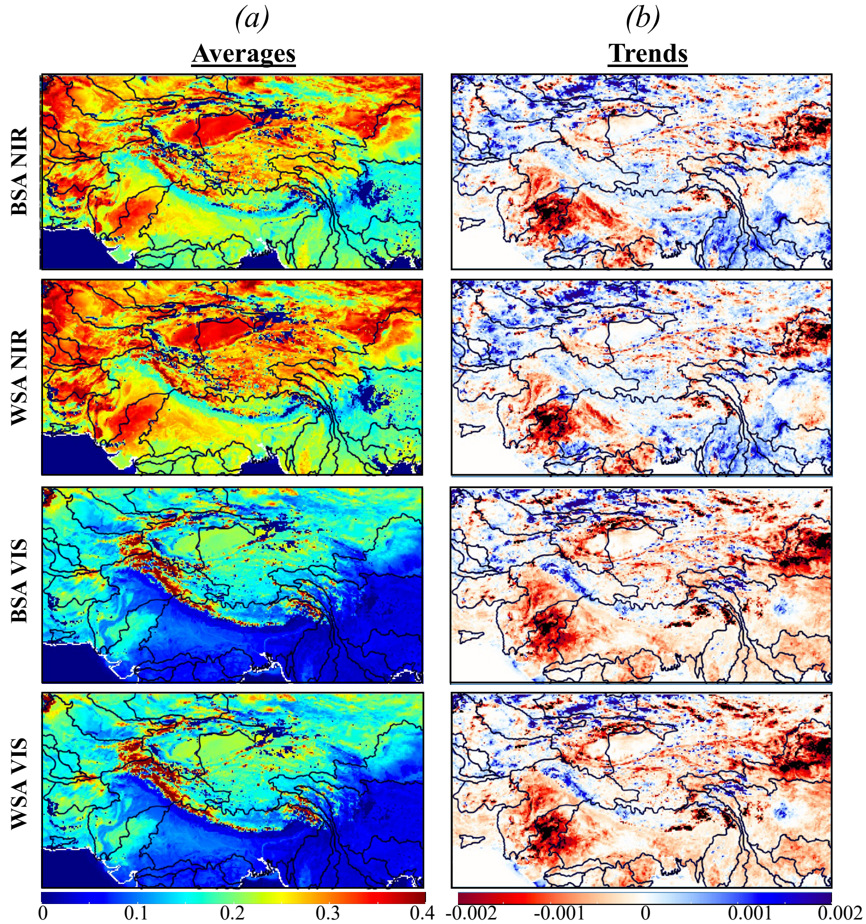

Figure 2: Surface albedo changes and values in High Mountain Asia. Spatial distributions of the yearly (a) averages and (b) trends from 2003 to 2020 of BSA (Black Sky) and WSA (White Sky) surface albedos in both NIR and VIS wavelengths. Trends were computed using the Mann-Kendall test with a confidence level of 95%.

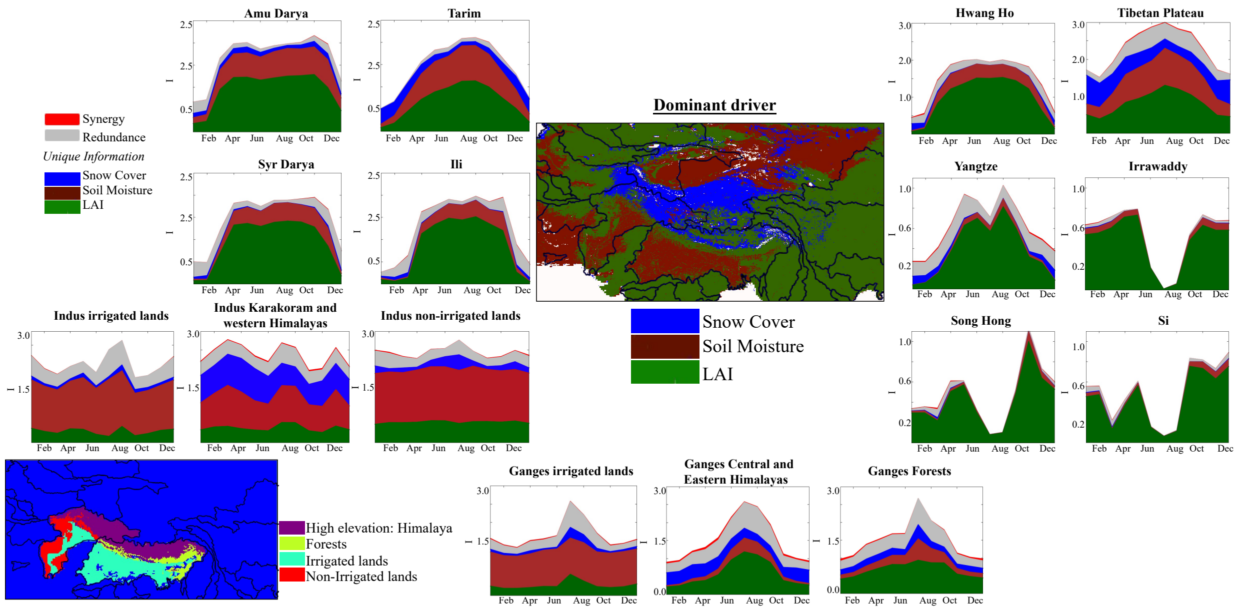

Figure 3: Dominant drivers of the surface albedo changes. Spatiotemporal variations of the unique and redundant information of leaf area index, soil moisture, and snow cover about the visible white-sky surface albedo of 16 zones (basin names are indicated in Figure 1c). Note that y-axis is a stacked graph and is not cumulative.

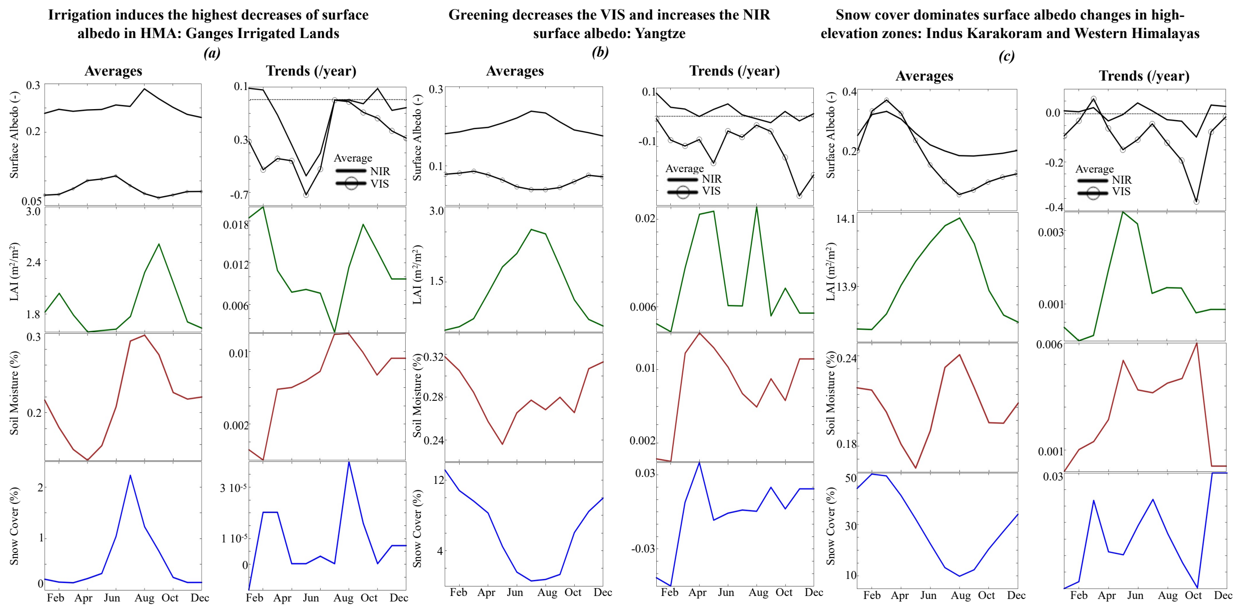

Figure 4: Monthly variations of trends and averages of surface albedo, LAI, soil moisture and snow cover. (a) in a basin where irrigation decreases surface albedo: irrigated lands of the Ganges-Brahmaputra, (b) in a basin where greening decreases VIS and increases NIR surface albedo: Yangtze, (c) in a basin where changes in snow cover decreases surface albedo: the Karakoram and Western Himalayas in the Indus. Trends were computed using the Mann-Kendall test with a confidence level of 95%.

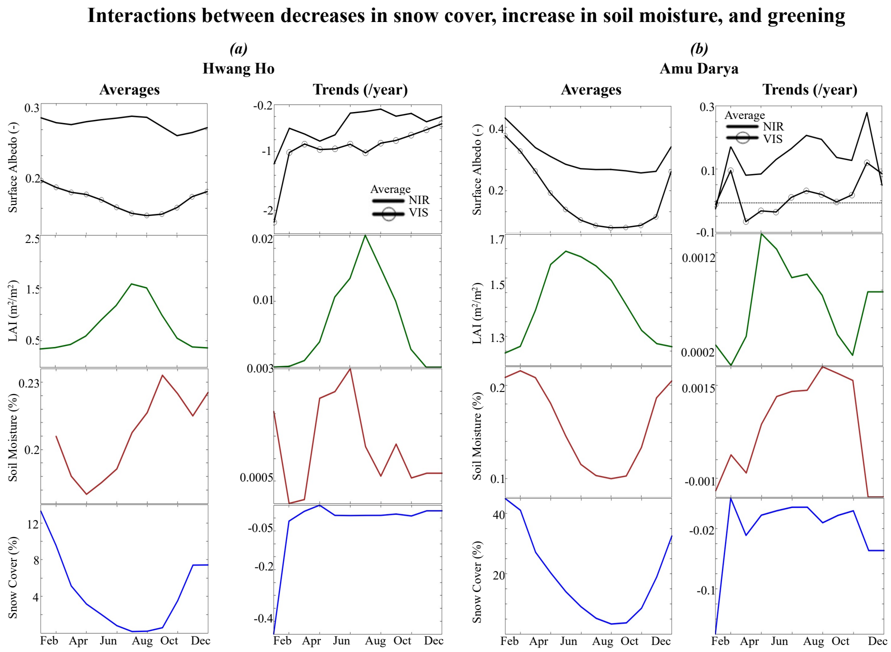

Figure 5: Monthly variations of trends and averages of surface albedo, LAI, soil moisture and snow cover in basins where surface albedo changes are controlled by greening, soil moisture, and snow cover (a) Hwang Ho, and (b) Amu Darya. Trends were computed using the Mann-Kendall test with a confidence level of 95%.

Supplementary Files

This is a list of supplementary files associated with this preprint. Click to download.

- SupplementaryInformation.pdf